Expression of hypoxia-inducible factor-1α and -2α in whole-mount prostate histology: Relation with dynamic contrast-enhanced MRI and Gleason score

ALIE BORREN[1], GREETJE GROENENDAAL[1], PETRA VAN DER GROEP[2], MAAIKE R. MOMAN[1], ARTO E. BOEKEN KRUGER[3], UULKE A. VAN DER HEIDE[1], TRUDY N. JONGES[2], PAUL J. VAN DIEST[2], MARCO VAN VULPEN[1] and MARIELLE E.P. PHILIPPENS[1]

Departments of [1]Radiotherapy, [2]Pathology and [3]Urology, University Medical Center Utrecht, Utrecht, The Netherlands

Received January 15, 2013; Accepted March 4, 2013

DOI: 10.3892/or.2013.2392

Abstract. The aim of this study was to investigate the association between the immunohistochemical expression of hypoxia-inducible factor (HIF)-1α and HIF-2α and dynamic contrast-enhanced magnetic resonance imaging (DCE-MRI) parameters K^{trans} and k_{ep} in prostate cancer. Therefore, 15 patients with biopsy-confirmed prostate cancer underwent a pre-operative 3T DCE-MRI scan. Immunohistochemical analysis of HIF-1α and HIF-2α, and of CD31 for microvessel density (MVD) was performed. Tumor areas were delineated on whole-mount histopathological sections. Nuclear HIF expression was correlated with the quantitative DCE-MRI parameters K^{trans} and k_{ep}, MVD and Gleason score. HIF expression was highly heterogeneous within tumors and between patients. Pronounced expression of HIF-2α was present, while HIF-1α expression was more limited. Larger tumors showed higher HIF-2α expression (P=0.041). A correlation between HIF-2α and K^{trans} $p5^{th}$ was found (r=0.30, P=0.02), but no differences in K^{trans}, k_{ep} and MVD were observed for different levels of HIF expression. HIF expression was not associated with Gleason score. In conclusion, in this whole-mount prostate cancer study, larger prostate tumors showed frequently high HIF-2α expression, suggesting that larger tumors are clinically most relevant. However, HIF-1α and HIF-2α were not correlated with DCE-MRI parameters. Given the pronounced expression of HIF-2α and independence of Gleason score, HIF expression may function as a biomarker to guide boost dose prescription.

Introduction

Biochemical failure and local recurrences of prostate cancer after radiotherapy could be reduced by escalation of the radiation dose to the prostate (1,2). As local recurrences frequently originate at the site of the macroscopic tumor, the focus for further dose escalation has to be on focal tumor areas most in need of aggressive treatment (3-5).

Based on recent studies, we know that hypoxia-inducible factor (HIF) may be related to prostate cancer outcome, as higher HIF expression was found to be associated with increased risk of biochemical failure and with reduced survival (6-8). Because of this relationship, tumor areas with high HIF expression may be candidates for focal boost.

HIF is a transcription factor which can be regulated by hypoxia-dependent and hypoxia-independent mechanisms. The hypoxia-dependent mechanism has been the most investigated; levels of HIFα subunits in the cell increase under hypoxic conditions resulting from an imbalance between oxygen demand and oxygen delivery to the tissue. In this pathway, HIF transcription factors act as key regulators of the cellular response to hypoxia and modulate the expression of genes involved in processes such as cell metabolism, proliferation and angiogenesis. The hypoxia-independent pathway of HIF-regulation is the induction of HIFα expression by increased oncogenic signaling in cancer cells (9). Most studies have focused on the presence of HIF-1α. However, HIF-2α may play an additional and important role in prostate cancer (8,9). The role of HIF-2α in prostate cancer is still underexposed and its distribution in whole-mount prostate histology not yet described. This is the first study describing the distribution of HIF-2α expression in whole-mount prostate histology.

For the non-invasive detection of prostate tumor areas, dynamic contrast-enhanced magnetic resonance imaging (DCE-MRI) is one of the tools currently used in clinical practice (10). The aim of the present study was to investigate the relation of the DCE-MRI parameters K^{trans} and k_{ep} with the immunohistochemical expression of HIF-1α and HIF-2α in whole-mount prostate histology.

Materials and methods

Patients. The study was approved by the Institutional Review Board of the University Medical Center Utrecht, and informed

Correspondence to: Dr Alie Borren, Department of Radiotherapy, University Medical Center Utrecht, Heidelberglaan 100, 3584 CX Utrecht, The Netherlands
E-mail: a.borren@umcutrecht.nl

Key words: HIF-1α, HIF-2α, prostate cancer, K^{trans}, k_{ep}

Table I. Patient characteristics.

Characteristics	Value
Patient no.	15
Patient age (years)[a]	63 (48-74)
PSA level (ng/ml)[a]	12 (5-29)
Pathological tumor stage[b]	
T2a	2
T2c	5
T3a	8
Gleason score[b]	
3+3=6	2
3+4=7	10
3+5=8	3
Tumor no.	34
<0.22 cm^3	14
>0.22 cm^3	20
Tumor volume[a]	0.73 (0.01-9.36)
<0.22 cm^3	0.17 (0.01-0.21)
>0.22 cm^3	1.59 (0.42-9.36)

[a]Median and (range). [b]Patient numbers.

consent was obtained from all patients. Twenty patients were enrolled in the study. All patients had biopsy-confirmed prostate cancer and were scheduled for a robotic-assisted laparoscopic prostatectomy (RALP). None of the patients was treated with androgen deprivation therapy. Five patients were excluded from analysis, due to the unavailability of pathological material in 2 patients, considerable motion during MR image acquisition in 1 patient, and in 2 patients the prostate specimen was severely deformed which hampered accurate registration. Clinical characteristics of the 15 eligible patients are shown in Table I.

MR imaging. Multi-parametric imaging was performed on a 3T MRI-scanner (Philips Achieva, Best, The Netherlands), including a T2w sequence and DCE-MRI. No endorectal coil was used. T2w images were acquired with a fast spin-echo sequence, TR/TE=8396/120 msec, echo train length 13, acquisition matrix 256x256, field of view (FOV)=20 cm, slice thickness 3 mm, slice gap 1 mm. The DCE-MRI protocol consisted of a 3D spoiled gradient echo sequence (20 transverse slices, 2.5-mm slice thickness, TR/TE=4.0/1.7 msec, flip angle 8˚, FOV=40 cm, acquisition matrix 160x128). Scans were repeated 120 times at 2.5-sec intervals. A concentration of 0.1 ml/kg of gadobutrol (1.0 M) (Gadovist®, Schering AG, Berlin, Germany) contrast was injected at 2 ml/sec, followed by a saline flush. The tracer kinetics data were analyzed with the Tofts model, as previously described (11). This yielded 3D absolute K^{trans} and k_{ep} parameter maps. A generic arterial input function (AIF) was used for all patients, due to measurement errors on the patient-specific input functions. To account for patient-specific differences in AIF, DCE-MRI parameters were normalized to the median value in normal PZ for correlation analyses (12).

MRI-pathology registration. After prostatectomy, the prostate specimens were processed and registered as previously described (12). In short, the prostate was cut into 3-mm thick slices, and whole-mount microscopic slices stained with hematoxylin and eosin (H&E) were created. Tumor areas were delineated by a pathologist and assigned with a Gleason score. The registration process was performed in three steps: i) reconstruction of the prostate from 3-mm macroscopic slices, ii) registration of microscopic slices to the reconstructed prostate, and iii) registration between the reconstructed prostate and the T2w MR images. On average, the registration error between MR images and histopathological data was approximately one voxel (reconstructed voxel size 2.5x2.5x2.5 mm^3) (12).

Immunohistochemistry. After deparaffination and rehydration, endogenous peroxidase was blocked and antigen retrieval was performed. For microvessel density analysis, slides were incubated for 1 h at room temperature with a monoclonal mouse anti-human CD31 antibody (1:50) (Leica Microsystems, Wetzlar, Germany). For HIF-1α and HIF-2α, slides were incubated overnight at 4˚C using a monoclonal mouse anti-human HIF-1α antibody (1:50) (BD Transduction Laboratories, Lexington, KY, USA) and a polyclonal rabbit anti-human HIF-2α antibody (1:700) (Novus Biologicals, Littleton, CO, USA), respectively. Subsequently, slides were incubated with a secondary antibody (CD31 and HIF-1α: Novolink Polymer Detection System; Leica Microsystems and HIF-2α: BrightVision; Immunologic, Duiven, The Netherlands). All slides were developed with diaminobenzidine followed by hematoxylin counterstaining.

Tissue evaluation. Three whole-mount microscopic slides per patient containing normal tissue, the index tumor and probable secondary tumors, were chosen for further analysis. CD31-stained slides were digitized at microscopic resolution and analyzed in ImageScope v10.0 using the Microvessel Analysis Algorithm v1 (Aperio Technologies, Vista, CA, USA) to assess the microvessel density (MVD). To compensate for variation in staining intensity, the settings of the algorithm were evaluated qualitatively and optimized for every batch by adjusting on test regions.

Scoring of HIF-1α and HIF-2α was performed by consensus of two observers. The percentage of positively stained nuclei in whole tumor regions was estimated per slide, ignoring diffuse cytoplasmic staining.

Regions of interest (ROIs) were defined based on the HIF-expression pattern. Areas within a tumor with a distinct HIF-expression pattern were investigated as separate regions, which could result in more regions of interest within a single tumor. This was carried out separately for HIF-1α and HIF-2α.

Statistical analysis. Median K^{trans}, k_{ep} and MVD were calculated for each ROI. For analysis of K^{trans}, k_{ep} and MVD, ROIs were selected within tumors with a volume >0.22 cm^3 (diameter >3 voxels = 7.5 mm), as partial volume effects and registration errors have a large influence on smaller tumors. Normalized DCE-MRI parameters were used for statistical analysis to

Table II. Distribution of HIF-1α and HIF-2α in patients and tumors.

		HIF-1α [n/total (%)]	HIF-2α [n/total (%)]
Patients	HIF-positive	12/15 (80)	14/15 (93)
Tumors			
Total	HIF-positive	20/34 (59)	28/34 (82)
<0.22 cm^3	HIF-positive	7/14 (50)	9/14 (64)
	Maximum HIF-expression[a]	20%	35%
>0.22 cm^3	HIF-positive	13/20 (65)	19/20 (95)
	Maximum HIF-expression[a]	50%	90%

HIF, hypoxia-inducible factor. [a]Percentage of tumor cells with positive staining.

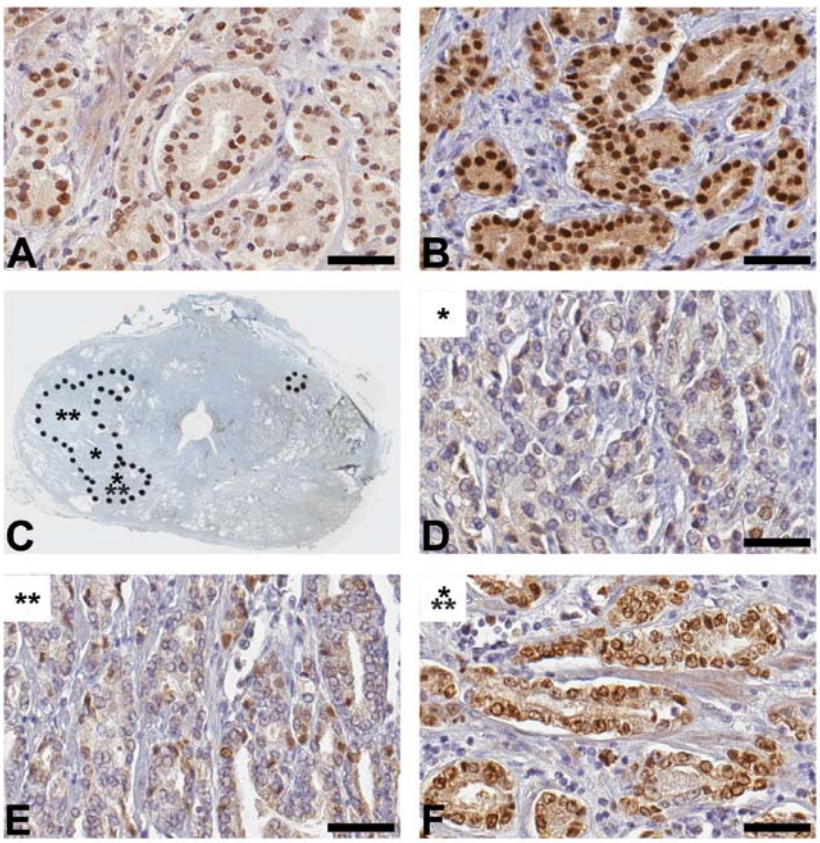

Figure 1. Example of (A) strong HIF-1α staining and (B) strong HIF-2α staining in the same patient. Second patient example showing the heterogeneity of HIF-2α expression within one tumor. (C) Overview of HIF-2α-positive areas with HIF-2α expression of (D) 5%, (E) 10% and (F) 90%. Scale bar, 50 μm.

account for interpatient variability. Differences between ROIs were assessed with the Mann-Whitney U and Kruskal-Wallis test, and Spearman's correlation coefficients were calculated (SPSS v20, SPSS Inc., Chicago, IL, USA). P-values ≤0.05 were considered to indicate statistically significant differences.

Results

Of the 15 patients, most showed HIF-1α and HIF-2α-positive tumor areas (Table II). The distribution of HIF expression was highly heterogeneous: i) negative and positive tumors were found within patients, ii) negative and positive areas were found within tumors, and iii) within a single tumor the range in HIF-positivity could be large with 5-35% for HIF-1α and 2-90% for HIF-2α. In Fig. 1, this heterogeneous distribution is illustrated for HIF-2α. Tumor areas showing HIF expression, could either be very small or comprise the entire tumor. There was a marked difference in the distribution of HIF-1α and HIF-2α. HIF-1α expression was often present focally in small regions within tumors, while HIF-2α frequently was expressed in whole tumor regions. Furthermore, the maximum HIF-1α expression was 50%, whereas HIF-2α ranged to 90%. HIF expression was sometimes found in normal tissue, but was not taken into account.

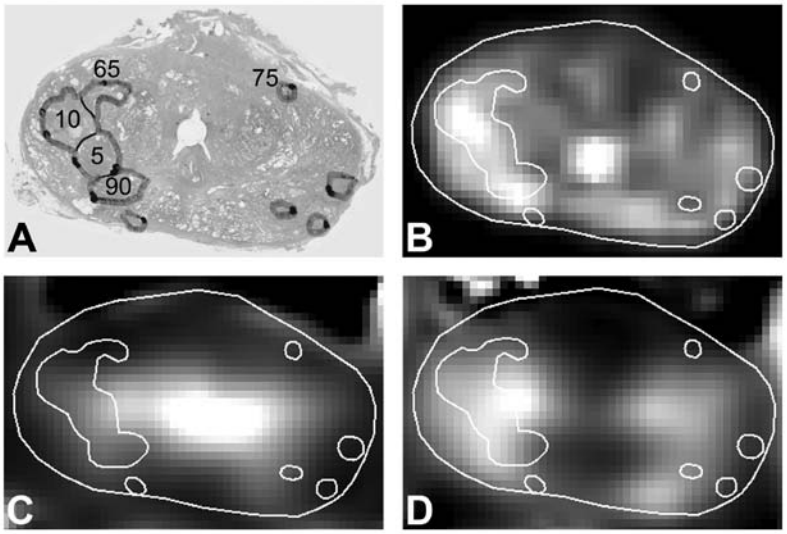

Figure 2. Patient example showing the absence of correlations between (A) percentages of HIF-2α expression and (B) K^{trans}, (C) k_{ep} and (D) MVD. HIF-1α expression in this patient was 0% in all tumor regions.

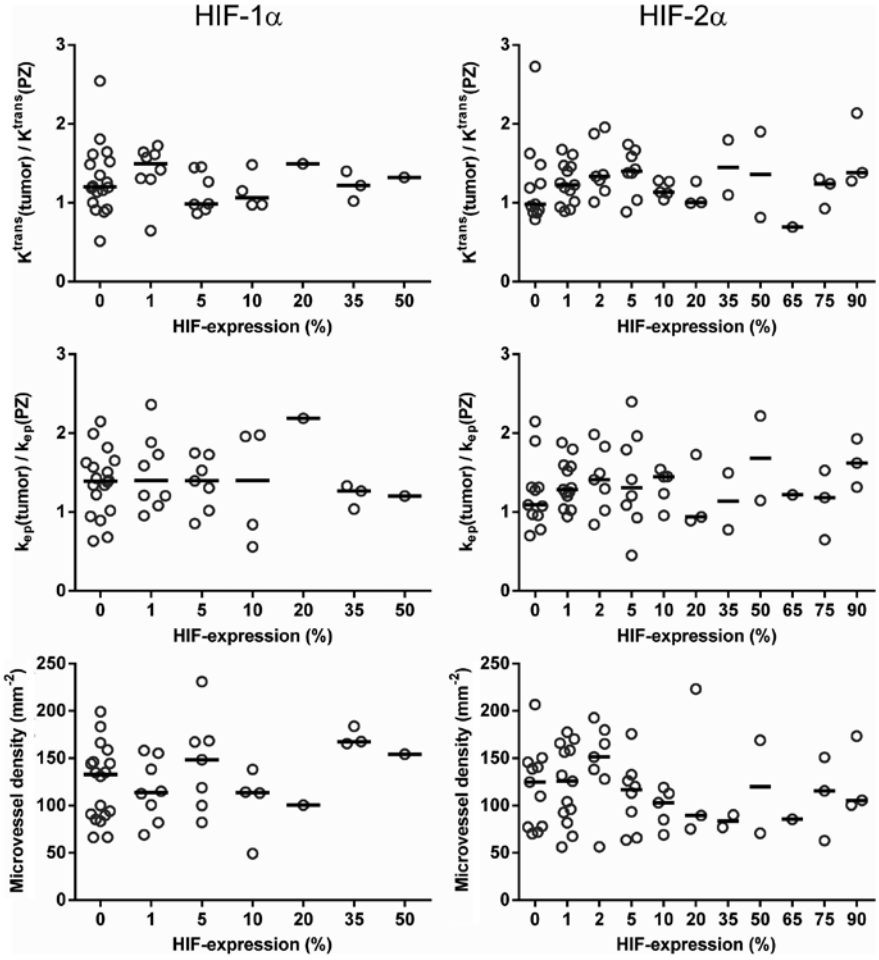

Figure 3. Graphs indicating the large heterogeneity of K^{trans}, k_{ep} and MVD for the different HIF-expression levels. Bar, median.

For all HIF-1α ROIs, median values (range) were: K^{trans} 0.241 min^{-1} (0.108-0.599), k_{ep} 0.356 min^{-1} (0.049-0.581) and MVD 135/mm^2 (50-230). For HIF-2α these values were: K^{trans} 0.256 min^{-1} (0.109-0.609), k_{ep} 0.362 (0.051-0.888) and MVD 115/mm^2 (55-225). No differences in median K^{trans}, k_{ep} and MVD were observed between different HIF-expression levels (Fig. 2). In addition, classification into groups according to different HIF-expression levels (e.g. HIF-positive vs.

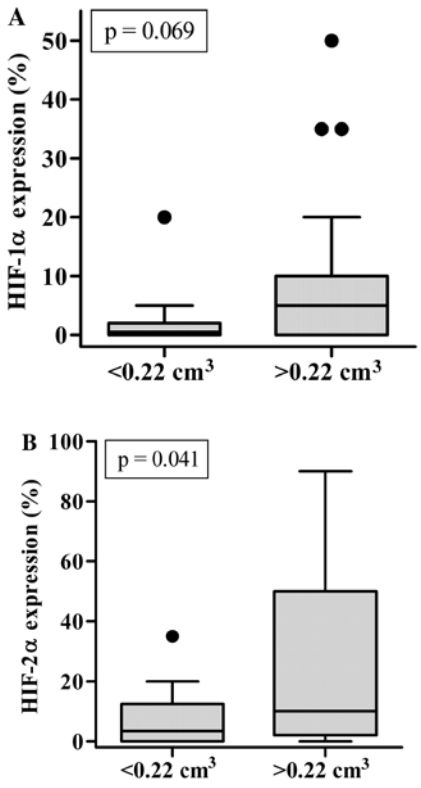

Figure 4. (A) HIF-1α and (B) HIF-2α expression vs. tumor volume.

HIF-negative and 0-1% vs. >1%) did not show any significant differences. As shown in Fig. 3, the perfusion parameters and MVD in HIF-negative tumor regions (with 0% HIF expression) overlapped with those in all other HIF-positive ROIs.

Furthermore, ROIs were classified into groups with high/low K^{trans} and high/low k_{ep}, using median normalized K^{trans} and k_{ep} values as threshold. No differences in HIF expression were present between the groups (P>0.16).

Percentages of HIF-1α and HIF-2α expression were not correlated with median K^{trans}, k_{ep} and MVD (P>0.2). HIF-2α expression was correlated with the K^{trans} 5th percentile (r=0.30, P=0.02) and with the MVD 95th percentile (r=-0.39, P=0.002). HIF-1α and HIF-2α were not correlated with each other (P=0.49) and both did not correlate with Gleason score (P>0.77).

Larger tumors (>0.22 cm^3) were more often HIF-2α-positive (P=0.023) than smaller tumors and showed higher levels of HIF-2α expression (P=0.041). This association of HIF expression with tumor volume was less clear for HIF-1α (Fig. 4). In addition, larger tumors showed more frequent presence of Gleason grade 4 (P=0.005), but for Gleason grade 5 no difference between smaller and larger tumors was observed (P=0.955).

Discussion

This is the first study describing the distribution of HIF-2α expression in whole-mount prostate histology. We described the distribution of nuclear HIF-1α and HIF-2α expression in prostate cancer and investigated the relationship with DCE-MRI parameters and MVD. HIF distribution was highly heterogeneous, with pronounced expression of HIF-2α, while HIF-1α was more limited.

To date, the presence of HIF-2α in primary prostate cancer has been described in regards to data of tissue microarrays only (8,13). Boddy *et al* (13) suggested that HIF-2α may be the most important isoform in prostate cancer, as they showed that HIF-2α expression was negatively correlated with the presence of prolyl hydroxylase enzyme PHD2. Under hypoxic conditions, this enzyme becomes inactive, with subsequent higher levels of HIF-2α. In the present study, we underscore this suggestion, as we found that the expression of HIF-2α was more pronounced and reached higher levels compared with HIF-1α.

In addition, we observed higher HIF-2α expression levels in larger tumors. In light of the prognostic relevance of HIF expression, this suggests that larger tumors are most clinically relevant. These larger tumors have a higher chance to be detected with MRI compared with smaller tumors (14). However, we found that high HIF expression was present as well in small tumor regions. Unfortunately, these small tumors may not be detected with MRI.

Furthermore, we observed a weak positive correlation between HIF-2α and the K^{trans} 5th percentile, which indicates that the minimum K^{trans} is higher in tumors with higher HIF-2α expression. This may facilitate tumor detection, as higher K^{trans} increases the conspicuity of tumor voxels (12).

Despite these encouraging results, we did not observe any differences and correlations between HIF expression and median DCE-MRI parameters or MVD. The question is whether HIF expression in prostate cancer is regulated in an hypoxia-dependent or hypoxia-independent manner. If hypoxia-dependent, HIF induces angiogenesis by upregulation of vascular endothelial growth factor. Therefore, we would expect high MVD and high K^{trans} in regions with high HIF expression. However, HIF expression may be induced by several non-hypoxia-related factors (15). In a recent study, Garcia-Parra *et al* (16) put a critical note on the association between HIF-1α expression and hypoxia. While they found variable HIF-1α staining, they were not able to show hypoxia in prostate cancer with ^{18}F-FAZA PET/CT or with immunohistochemical staining of CAIX which is a downstream target of HIF-1α. Based on these findings, they suggest that the expression of HIF-1α may be independent of tissue hypoxia.

Hypoxia-independence of HIF expression may clarify why we did not observe a correlation between HIF expression and DCE-MRI parameters and MVD.

For both HIF-1α and HIF-2α, a number of studies have shown an inverse relationship between HIF expression and biochemical recurrence (6-8). This prognostic value of HIF expression appears to be independent of the Gleason score. Similar to other reports, we did not find a correlation between expression of HIF-1α or HIF-2α and Gleason score (6,13,16). Therefore, HIF expression in prostate tumor biopsies may be used as input for individual boost dose prescription, to achieve personalized radiotherapy (17).

This study has some limitations. First, the number of patients was relatively small. Definitive conclusions on the relationship between HIF expression and DCE-MRI must be verified in larger studies. Nevertheless, as in this study the P-values found with correlation analyses were far from signifi-

cance, clinical relevant correlations might be absent as well in larger cohorts. Second, although we used a robust registration method, a registration error existed between DCE-MRI data and pathology.

In conclusion, in the present study we demonstrated that expression of HIF-1α and HIF-2α is not correlated with DCE-MRI parameters. Larger tumors showed frequently high HIF-2α expression, which suggests that larger tumors are most clinically relevant tumors. Given the pronounced expression of HIF-2α and independence of Gleason score, HIF expression may function as a biomarker to guide boost dose prescription.

References

1. Peeters ST, Heemsbergen WD, Koper PC, *et al*: Dose-response in radiotherapy for localized prostate cancer: results of the Dutch multicenter randomized phase III trial comparing 68 Gy of radiotherapy with 78 Gy. J Clin Oncol 24: 1990-1996, 2006.
2. Zelefsky MJ, Pei X, Chou JF, *et al*: Dose escalation for prostate cancer radiotherapy: predictors of long-term biochemical tumor control and distant metastases-free survival outcomes. Eur Urol 60: 1133-1139, 2011.
3. Cellini N, Morganti AG, Mattiucci GC, *et al*: Analysis of intraprostatic failures in patients treated with hormonal therapy and radiotherapy: implications for conformal therapy planning. Int J Radiat Oncol Biol Phys 53: 595-599, 2002.
4. Pucar D, Hricak H, Shukla-Dave A, *et al*: Clinically significant prostate cancer local recurrence after radiation therapy occurs at the site of primary tumor: magnetic resonance imaging and step-section pathology evidence. Int J Radiat Oncol Biol Phys 69: 62-69, 2007.
5. Lips IM, van der Heide UA, Haustermans K, *et al*: Single blind randomized Phase III trial to investigate the benefit of a focal lesion ablative microboost in prostate cancer (FLAME-trial): study protocol for a randomized controlled trial. Trials 12: 255, 2011.
6. Vergis R, Corbishley CM, Norman AR, *et al*: Intrinsic markers of tumour hypoxia and angiogenesis in localised prostate cancer and outcome of radical treatment: a retrospective analysis of two randomised radiotherapy trials and one surgical cohort study. Lancet Oncol 9: 342-351, 2008.
7. Gravdal K, Halvorsen OJ, Haukaas SA, *et al*: Proliferation of immature tumor vessels is a novel marker of clinical progression in prostate cancer. Cancer Res 69: 4708-4715, 2009.
8. Nanni S, Benvenuti V, Grasselli A, *et al*: Endothelial NOS, estrogen receptor beta, and HIFs cooperate in the activation of a prognostic transcriptional pattern in aggressive human prostate cancer. J Clin Invest 119: 1093-1108, 2009.
9. Keith B, Johnson RS and Simon MC: HIF1α and HIF2α: sibling rivalry in hypoxic tumour growth and progression. Nat Rev Cancer 12: 9-22, 2011.
10. Futterer JJ, Heijmink SW, Scheenen TW, *et al*: Prostate cancer localization with dynamic contrast-enhanced MR imaging and proton MR spectroscopic imaging. Radiology 241: 449-458, 2006.
11. Groenendaal G, Moman MR, Korporaal JG, *et al*: Validation of functional imaging with pathology for tumor delineation in the prostate. Radiother Oncol 94: 145-150, 2010.
12. Groenendaal G, Borren A, Moman MR, *et al*: Pathologic validation of a model based on diffusion-weighted imaging and dynamic contrast-enhanced magnetic resonance imaging for tumor delineation in the prostate peripheral zone. Int J Radiat Oncol Biol Phys 82: e537-e544, 2012.
13. Boddy JL, Fox SB, Han C, *et al*: The androgen receptor is significantly associated with vascular endothelial growth factor and hypoxia sensing via hypoxia-inducible factors HIF-1a, HIF-2a, and the prolyl hydroxylases in human prostate cancer. Clin Cancer Res 11: 7658-7663, 2005.
14. Roethke MC, Lichy MP, Jurgschat L, *et al*: Tumorsize dependent detection rate of endorectal MRI of prostate cancer, a histopathologic correlation with whole-mount sections in 70 patients with prostate cancer. Eur J Radiol 79: 189-195, 2011.
15. Banham AH, Boddy J, Launchbury R, *et al*: Expression of the forkhead transcription factor FOXP1 is associated both with hypoxia inducible factors (HIFs) and the androgen receptor in prostate cancer but is not directly regulated by androgens or hypoxia. Prostate 67: 1091-1098, 2007.
16. Garcia-Parra R, Wood D, Shah RB, *et al*: Investigation on tumor hypoxia in resectable primary prostate cancer as demonstrated by ^{18}F-FAZA PET/CT utilizing multimodality fusion techniques. Eur J Nucl Med Mol Imaging 38: 1816-1823, 2011.
17. Bentzen SM and Gregoire V: Molecular imaging-based dose painting: a novel paradigm for radiation therapy prescription. Semin Radiat Oncol 21: 101-110, 2011.